Scientific Journal of Silesian University of Technology. Series Transport
Zeszyty Naukowe Politechniki Śląskiej. Seria Transport

Volume 90 **2016**

p-ISSN: 0209-3324

e-ISSN: 2450-1549

DOI: 10.20858/sjsutst.2016.90.11

Journal homepage: http://sjsutst.polsl.pl

Article citation info:
Kolarič, D., Kolarič, M. Example of flow modelling characteristics in diesel engine nozzle. *Scientific Journal of Silesian University of Technology. Series Transport*. 2016, **90**, 123-135. ISSN: 0209-3324. DOI: 10.20858/sjsutst.2016.90.11.

Dušan KOLARIČ[1], Marko KOLARIČ[2]

EXAMPLE OF FLOW MODELLING CHARACTERISTICS IN DIESEL ENGINE NOZZLE

Summary. Modern transport is still based on vehicles powered by internal combustion engines. Due to stricter ecological requirements, the designers of engines are continually challenged to develop more environmentally friendly engines with the same power and performance. Unfortunately, there are not any significant novelties and innovations available at present which could significantly change the current direction of the development of this type of propulsion machines. That is why the existing ones should be continually developed and improved or optimized their performance. By optimizing, we tend to minimize fuel consumption and lower exhaust emissions in order to meet the norms defined by standards (i.e. Euro standards). Those propulsion engines are actually developed to such extent that our current thinking will not be able to change their basic functionality, but possible opportunities for improvement, especially the improvement of individual components, could be introduced. The latter is possible by computational fluid dynamics (CFD) which can relatively quickly and inexpensively produce calculations prior to prototyping and implementation of accurate measurements on the prototype. This is especially useful in early stages of development or at optimization of dimensional small parts of the object where the physical execution of measurements is impossible or very difficult. With advances of computational fluid dynamics, the studies on the nozzles and outlet channel injectors have been relieved. Recently, the observation and better understanding of the flow in nozzles at large pressure

[1] Vocational College of Traffic and Transport Maribor, Preradovičeva 33, 2000 Maribor, Slovenia. E-mail: dusan.kolaric@guest.arnes.si.
[2] Vocational College of Traffic and Transport Maribor, Preradovičeva 33, 2000 Maribor, Slovenia. E-mail: dusan.kolaric@guest.arnes.si.

and high velocity is recently being possible. This is very important because the injection process, especially the dispersion of jet fuel, is crucial for the combustion process in the cylinder and consequently for the composition of exhaust gases. And finally, the chemical composition of the fuel has a strong impact on the formation of dangerous emissions, too. The research presents the influence of various volume mesh types on flow characteristics inside a fuel injector nozzle. Our work is based upon the creating of two meshes in the CFD software package. Each of them was used two times. First, a time-dependent mass flow rate was defined at the inlet region and pressure was defined at the outlet. The same mesh was later used to perform a simulation with a defined needle lift curve (and hereby the mesh movement) and inlet and outlet pressure. In next few steps we investigated which approach offered better results and would thus be most suitable for engineering usage.

Keywords: diesel engine, mass flow, CFD, needle lift, injector, volume mesh

1. INTRODUCTION

The development of modern diesel engines is directed to increase capacity and lower consumption. In future, it will be especially oriented towards even greater fuel economy and purity of diesel engines. Therefore, more and more manufacturers tend to develop engines with smaller volumes, less cylinders and different systems for exhaust gas treatment.

In achieving these goals, fuel injection systems play an important role, since they are responsible for just-in-time and regular supply of fuel to the engine cylinders. In the course of time, there were several changes in their operation but the basic characteristics remain the same until today. Increased awareness for the environmental protection compel manufacturers to develop ever better and more efficient fuel injection systems. The latest are electronically controlled and allow precise control by opening and closing of valves, fuel injection time is shorter while injection pressure is significantly higher. Electronically controlled injection systems help to reduce harmful emissions (NO_X, soot) in the exhaust gases and to increase the engine power as well as reduce the level of noise.

Such systems allow the injection under high pressure (about 1500 to 2000 bars) which reduces the emissions of solid particles. The higher the pressure, the better the dispersion (smaller droplets) of the fuel is, which leads to better prepared mixtures at the same time. By controlling the injection pressure that depend on the load and engine frequency, these systems allow control of gaseous emissions and noise. For simultaneous reduction of NO_X and soot emissions, the optimal angle of starting injection time is important. The latter is important due to the interaction of different measures to reduce emissions of soot and NO_X. In turn, by reducing certain emissions, these measures often cause the increase of others. The injection with common rail allows all the above requirements [1].

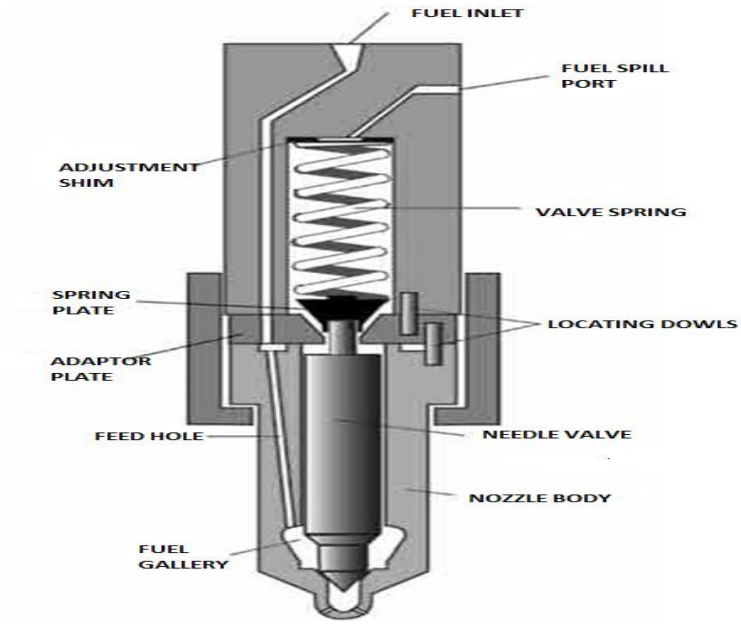

Fig. 1. Injector

The space, in which combustion takes place, and the system of fuel supply are connected by the injector nozzle, which is one of the most important elements of the fuel injection system. It is used at the end of the compression phase to enable the supply of fuel under high pressure to the combustion chamber. Injector nozzles take care of properly atomized fuel, which is essential for good combustion, low fuel consumption and the lowest emissions possible. Individual values of by-products of combustion also depend on pressure of fuel injection, openness of nozzles and valves, fuel characteristics and steering components [1].

Due to increased efficiency of the process, several different versions of nozzles have been developed. Their common task is to inject fuel into the cylinder of engine at optimum dispersion [2].

2. DESCRIPTION OF EXPERIMENT

2.1. Computer fluid dynamics (CFD)

Computers have become an indispensable part of modern engineering practice. By using computers, we can develop, design and improve old products faster. In the sixties, the development of computer fluid dynamics has started. Its main advantages, compared to conventional laboratory experiments, are the speed of implementation, easy adaptability and lower price. Consequently, many prototypes have not been required due to simulation which can figure out whether something is going to work or not and can be improved by the use of computer. For the purposes of CFD, there are several different software packages. In our case, the program, which is widely used in the automotive industry, was used for numerical simulation of our problem. The program is based on the finite volume method to analyze fluid flow [2].

2.2. Mathematical model of multiphase fluid flow in the selected CFD package

The object of our research is the numerical analysis of simultaneous flow of two fluid phases (vapor and liquid) through the injector of the fuel injection system. In order to solve such a mathematical-physical model, it is necessary to solve a system of conservation equations for each liquid phase separately.

The multiphase model describes each of the phases separately. The conservation equations for each phase are connected with terms that describe the transfer of mass, momentum, energy, turbulent kinetic energy and dissipation of turbulent kinetic energy. These terms are the weakest point of the multiphase model. In the Eulerian multiphase flow model, different equations are separately numerically solved for each of the two phases (*k* and *l*) in the model [3].

Mass conservation:

$$\frac{\partial \alpha_k \rho_k}{\partial t} + \nabla \cdot \alpha_k \rho_k \mathbf{v}_k = \sum_{l=1, l \neq k}^{n} \Gamma_{kl} \tag{1}$$

Here: ρ_k – density of phase k, α_k – volume fraction of phase k, v_k – velocity of phase k, Γ_{kl} – represents the interfacial mass exchange between phases *k* and *l*.

Here the following condition must be fulfilled:

$$\sum_{k=1}^{n} \alpha_k = 1 \tag{2}$$

Momentum conservation:

$$\frac{\partial \alpha_k \rho_k \mathbf{v}_k}{\partial t} + \nabla \cdot \alpha_k \rho_k \mathbf{v}_k \mathbf{v}_k = -\alpha_k \nabla p + \nabla \alpha_k \left(\boldsymbol{\tau}_k + \mathbf{T}_k^t \right) + \alpha_k \rho_k \mathbf{f} + \sum_{i=1, l \neq k}^{n} \mathbf{M}_{kl} + \mathbf{v}_k \sum_{l=1, l \neq k}^{n} \Gamma_{kl} \tag{3}$$

Here: $\mathbf{f}$ – body force vector which comprises gravity $\mathbf{g}$ and the inertial force in rotational frame, p – pressure (values of pressure are supposed to be equal for all phases), $\mathbf{M}_{kl}$ – term which presents the momentum interfacial interaction between phases *k* in *l*.

The shear stress $\boldsymbol{\tau}_k$ of the *k* phase is:

$$\boldsymbol{\tau}_k = \mu_k \left[\left(\nabla \mathbf{v}_k + \nabla \mathbf{v}_k^T \right) - \frac{2}{3} \nabla \cdot \mathbf{v}_k \right] \tag{4}$$

Reynolds stress $\mathbf{T}_k^t$ is:

$$\mathbf{T}_k^t = -\rho_k \overline{\mathbf{v}_k' \mathbf{v}_k'} = \mu_k^t \left[\left(\nabla \mathbf{v}_k + \nabla \mathbf{v}_k^T \right) - \frac{2}{3} \nabla \cdot \mathbf{v}_k \mathbf{I} \right] - \frac{2}{3} \rho_k k_k \mathbf{I} \tag{5}$$

Here: μ_k – molecular viscosity, μ_k^t – turbulent viscosity

Turbulent viscosity is modelled by:

$$\mu_k^t = \rho_k C_\mu \frac{k_k^2}{\varepsilon_k} \tag{6}$$

Energy (total enthalpy) conservation:

$$\begin{aligned}&\frac{\partial \alpha_k \rho_k h_k}{\partial t} + \nabla \cdot \alpha_k \rho_k \mathbf{v}_k h_k = \nabla \cdot \alpha_k \left(\mathbf{q}_k + \mathbf{q}_k^t\right) + \alpha_k \rho_k q_k''' + \alpha_k \rho_k \mathbf{f} \cdot \mathbf{v}_k + \\ &+ \nabla \cdot \alpha_k \left(\tau_k + \tau_k^t\right) \cdot \mathbf{v}_k + \alpha_k \frac{\partial p}{\partial t} + \sum_{l=1, l\neq k}^{n} \mathbf{H}_{kl} + h_k \sum_{l=1, l\neq k}^{n} \Gamma_{kl}\end{aligned} \tag{7}$$

Here: q_k''' – heat (entalpy) source, $\mathbf{H}_{kl}$ – represents the exchange of enthalpy between phases *k* and *l*; h_k – enthalpy of phase *k;* $\mathbf{q}_k$ – heat flux.

Heath flux $\mathbf{q}_k$ is defined by:

$$\mathbf{q}_k = \frac{\kappa_k}{c_{p,k}} \nabla h_k \tag{8}$$

Here: κ_k – thermal conductivity of phase *k*

Turbulent heat flux $\mathbf{q}_k^t$:

$$\mathbf{q}_k^t = -q_k \overline{v_k' h_k'} = \frac{\mu_k^t}{\sigma_k} \nabla h_k \tag{9}$$

Turbulent kinetic energy conservation:

$$\frac{\partial \alpha_k \rho_k k_k}{\partial t} + \nabla \cdot \alpha_k \rho_k \mathbf{v}_k k_k = \nabla \alpha_k \left(\mu_k + \frac{\mu_k^t}{\sigma_k}\right) \nabla k_k + \alpha_k P_k - \alpha_k \rho_k \varepsilon_k + \sum_{i=1, l\neq k}^{n} K_{kl} + h_k \sum_{i=1, l\neq k}^{n} \Gamma_{kl} \tag{10}$$

The production term due to shear, P_k, for phase k is:

$$P_k = \mathbf{T}_k^t : \nabla \mathbf{v}_k \tag{11}$$

Turbulent dissipation equation: [4, 5]

$$\begin{aligned}&\frac{\partial \alpha_k \rho_k \varepsilon_k}{\partial t} + \nabla \cdot \alpha_k \rho_k \mathbf{v}_k \varepsilon_k = \nabla \alpha_k \left(\mu_k + \frac{\mu_k^t}{\sigma_\varepsilon}\right) \nabla \varepsilon_k + \alpha_k C_1 P_k \frac{\varepsilon_k}{k_k} - \alpha_k C_2 \rho_k \frac{e_k^2}{k_k} + \\ &+ \alpha_k C_4 \rho_k \varepsilon_k \nabla \cdot \mathbf{v}_k + \sum_{i=1, l\neq k}^{n} D_{kl} + \varepsilon_k \sum_{i=1, l\neq k}^{n} \Gamma_{kl}\end{aligned} \tag{12}$$

Specifying mass transfer (mass interfacial exchange): the linear cavitation model was used. It based on the following relation for the mass exchange:

$$\Gamma_C = \rho_d N''' 4\pi R^2 \dot{R} = -\Gamma_d \tag{13}$$

Where: Γ – mass transfer, N''' – bubble number density, R – radius of bubbles.

2.3. Data for numerical calculation

Entry data for the calculation were obtained by measurements which were carried out in laboratory of engines on Friedmann & Maier device for testing outside vehicle injection systems. By using this device, data about the fuel mass flow and needle lift were collected and were used as boundary conditions in the simulation. They are presented in Figure 2.

TIME [s]	MASS FLOW [g/s]	TIME [s]	MASS FLOW [g/s]
0	0	0,0012	64,39
7,50E-05	19,9	0,001275	65,56
0,00015	32,19	0,00135	67,9
0,000225	40,97	0,001425	69,07
0,0003	48	0,0015	69,65
0,000375	50,34	0,001575	68,48
0,00045	51,51	0,00165	65,56
0,000525	52,68	0,001725	61,46
0,0006	55,02	0,0018	55,02
0,000675	56,78	0,001875	46,83
0,00075	58,53	0,00195	37,46
0,000825	59,12	0,002025	29,85
0,0009	60,29	0,0021	25,75
0,000975	62,05	0,002175	22,83
0,00105	63,22	0,00225	16,39
0,001125	63,8	0,002325	0

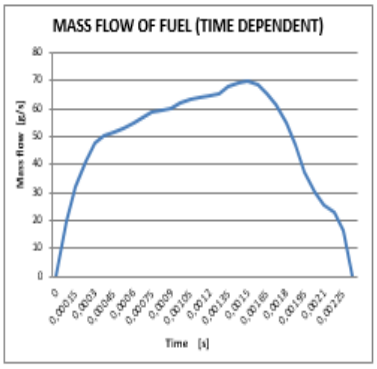

CRANCK ANGLE [°]	NEEDLE LIFT [mm]
0	0
150	0,01
156	0,3
166	0,3
170	0,01
360	0

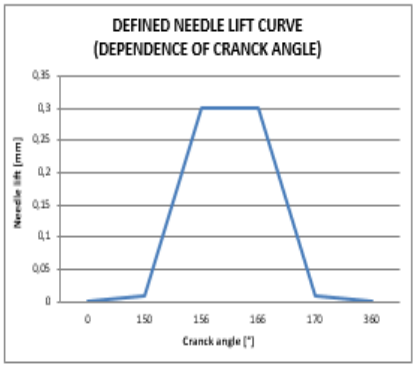

Fig. 2. Data about the fuel mass flow (left) and needle movement (right)

The measurement was performed on the Bosch nozzle, type DLL 25 S 834, which is used in the engine of MAN D2566 MUM. The pressure of needle lift is 175 bars, the maximum lift of the needle is 0.3 mm. It has a bore diameter d_n = 0.68 mm.

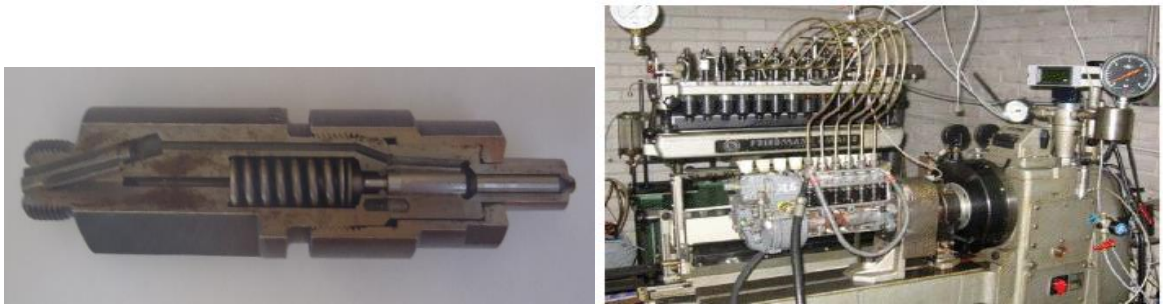

Fig. 3. Examined injector (left) and Friedmann & Maier device for injection testing systems (right)

2.4. Model mesh

The simulation was carried out on the geometric model of the extreme lower part of the injector, which covers the tip of the needle, seat area and bore for fuel injection (flow out channel). The geometrical model was formed from the 2D structure in Figure 4 (left). For the purpose of numerical simulations, there were created two spatial meshes on the model, consisting of 250.000 (mesh 1) and 400.000 (mesh 2) elements. At each mesh there were conducted two simulations: the one with defined mass flow and the one with defined needle lift (Figure 4, right).

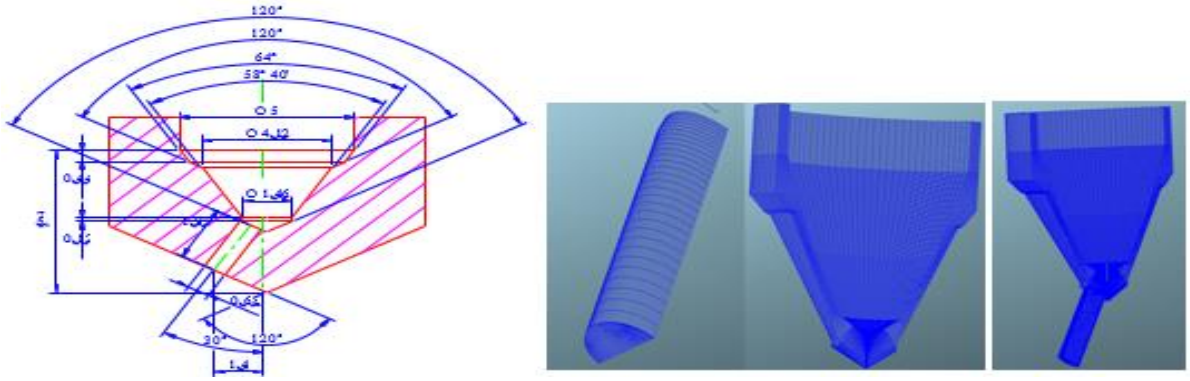

Fig. 4. Injector construction (left) and model mesh (injector body, fuel injection bore, combined in one body)

2.5. Boundary conditions of the model

The basic surfaces (selections) of the model are: inlet, outlet and symmetry. For each of them boundary conditions for multiphase flow were set. Furthermore, the parameters for controlling the calculation, defining characteristics of the fuel, and convergence criteria and parameters for postprocessing were determined.

In case of calculating the defined needle movement, the type of simulation "crank-angle" was used, which allows the change of conditions depending on crank angle. Therefore, for the performance of these simulations, besides the three already defined (Figure 5, left), 4 new selections were created: Needle_move, Buffer, Interpolation and No_move (Figure 5, right).

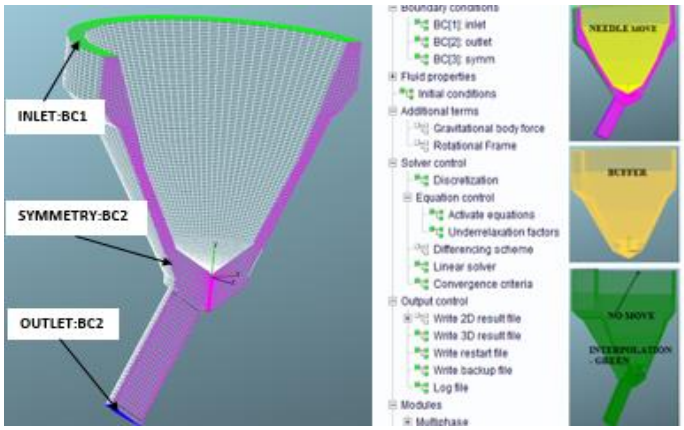

Fig. 5. Selections of boundary conditions (left), operational tree, additional selections of boundary conditions in case of defined needle movement (right)

3. ANALYZING RESEARCH RESULTS

The review of results included the analysis of velocity, turbulent kinetic energy and volume fraction in the outlet. Simulated values of the flow characteristics for both of the meshes and for both approaches at the flow inlet and outlet are introduced below. Examples illustrate the results after 0.001125 s of simulation (about half of the process).

3.1. Velocity

The comparability of meshes for both phases is relatively good in profile shape terms, but is very different in absolute terms. As shown in the graphs, the calculated values for the two phases are very similar at both the inlet and the outlet. However, the difference between both approaches is substantial. The results match better at the inlet to the bore. The values obtained with the defined needle movement seem more realistic.

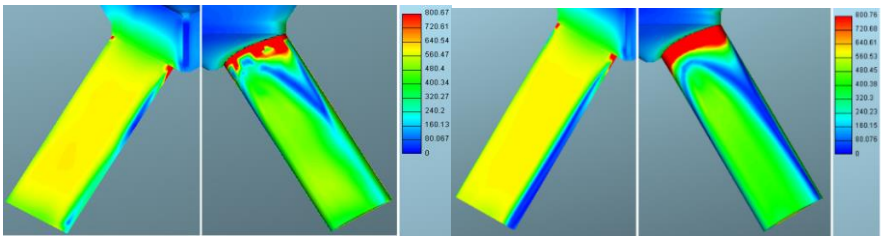

Fig. 6. Defined mass flow: velocities of gaseous phase for mesh 1 (left) and mesh 2 (right) in m/s

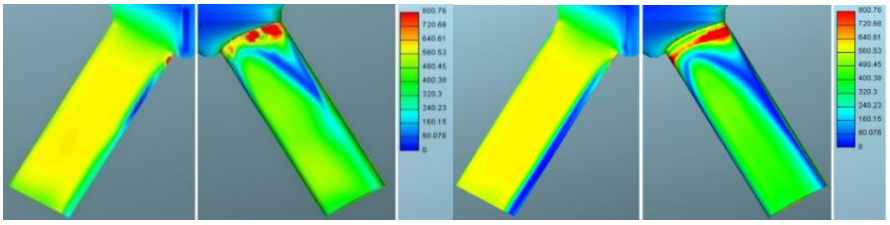

Fig. 7. Defined mass flow: velocities of liquid phase for mesh 1 (left) and mesh 2 (right) in m/s

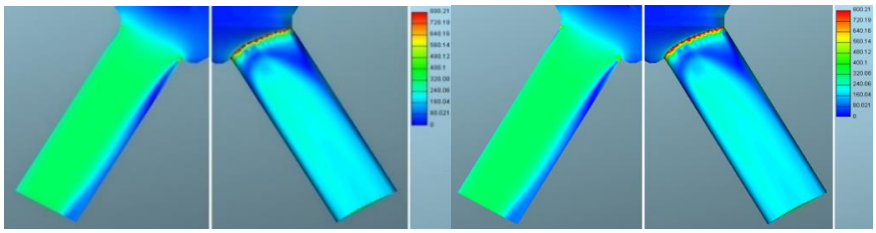

Fig. 8. Defined needle lift: velocities of gaseous phase for mesh 1 (left) and mesh 2 (right) in m/s

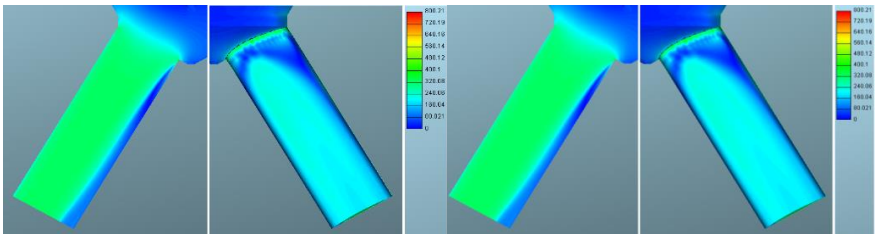

Fig. 9. Defined needle lift: velocities of liquid phase for mesh 1 (left) and mesh 2 (right) in m/s

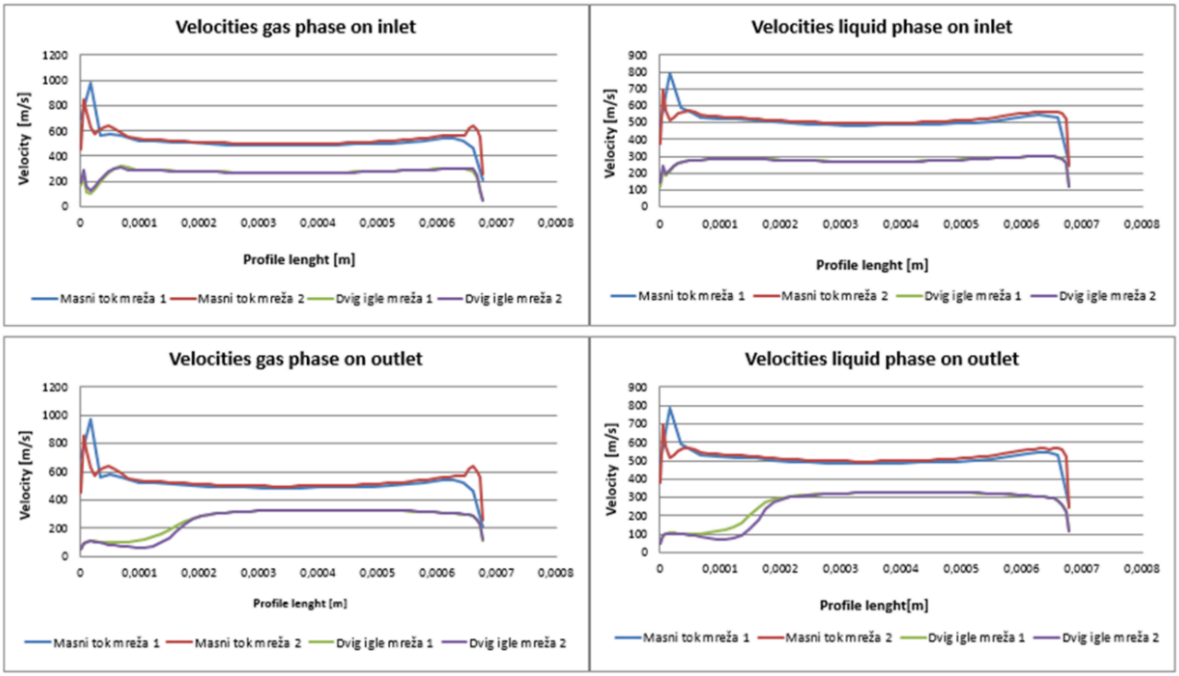

Fig. 10. Comparison of velocity profiles: Gaseous phase (left) – defined mass flow for meshes 1 and 2 and the defined needle lift for meshes 1 and 2; Liquid phase (right) – defined mass flow for meshes 1 and 2 and the defined needle lift for meshes 1 and 2

3.2. Turbulence kinetic energy

The comparison of results between the two meshes shows that the results of TKE are relatively well matched, and that there are only noticeable differences along the walls, while after that the flows subside. Slightly larger deviation is observed in the gaseous phase at the exit of the hole which is confirmed by the graphs of numerical values. The mesh density seems to have made a large impact on both approaches.

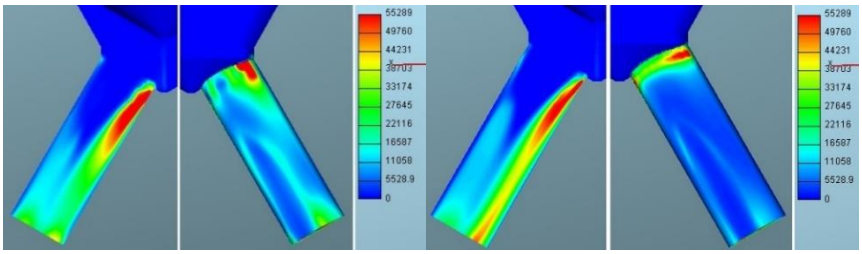

Fig. 11. Defined mass flow: Turbulence kinetic energy of gaseous phase for mesh 1 (left) and mesh 2 (right) in m^2/s^2

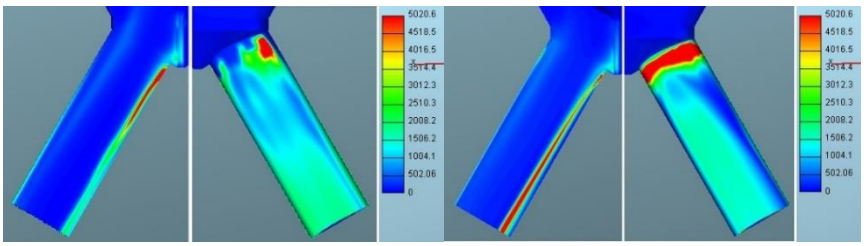

Fig. 12. Defined mass flow: Turbulence kinetic energy of liquid phase for mesh 1 (left) and mesh 2 (right) in m^2/s^2

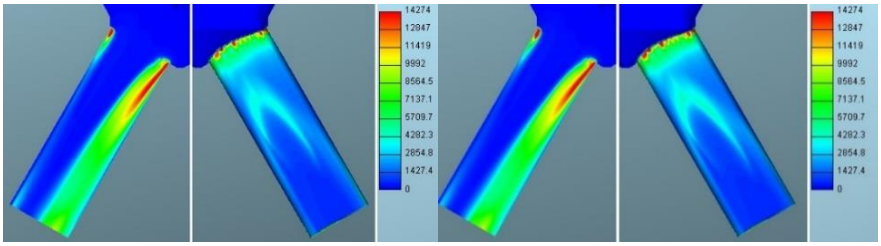

Fig. 13. Defined needle lift: Turbulence kinetic energy of gaseous phase for mesh 1 (left) and mesh 2 (right) in m^2/s^2

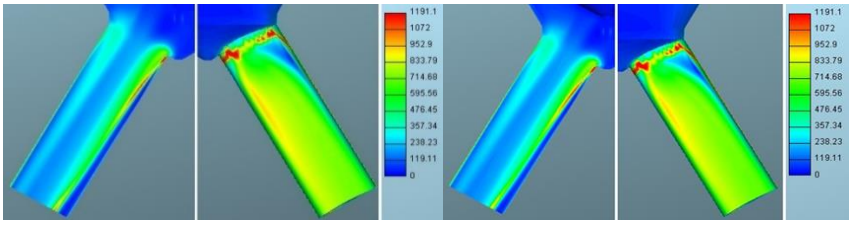

Fig. 14. Defined needle lift: Turbulence kinetic energy of liquid phase for mesh 1 (left) and mesh 2 (right) in m^2/s^2

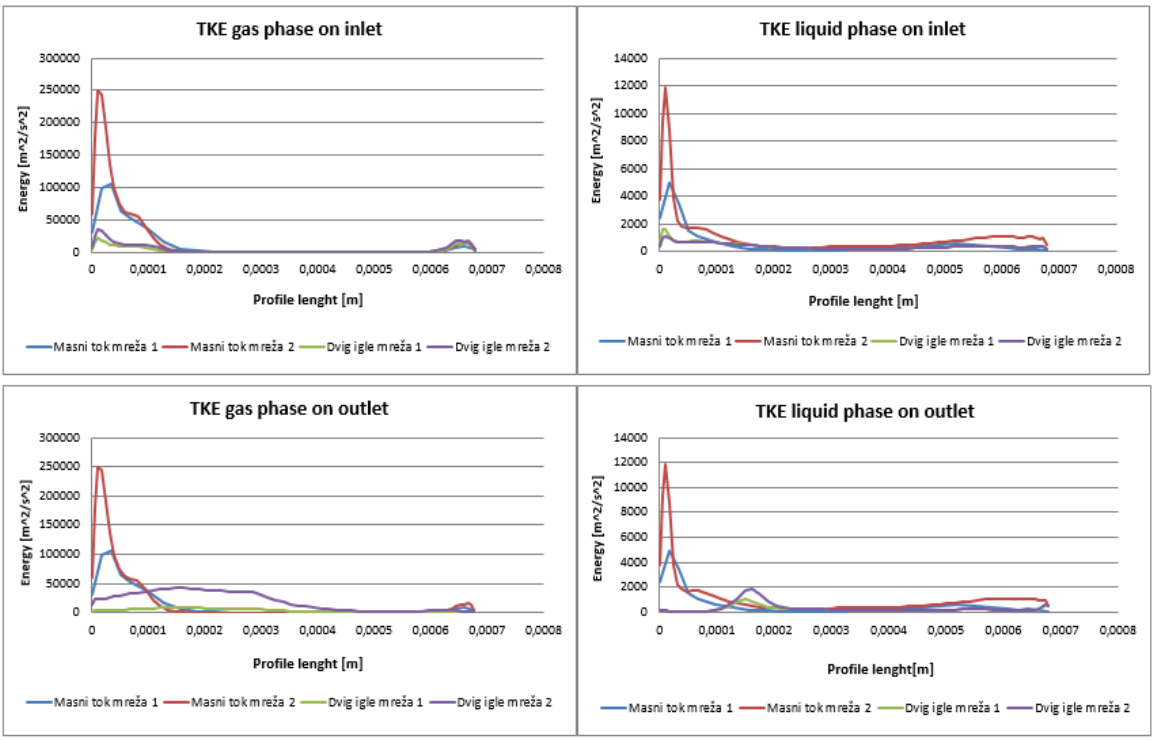

Fig. 15. The comparison of Turbulence kinetic energy (defined mass flow and needle lift - meshes 1 and 2)

3.3. Volume fraction

The volume fractions match well at the inlet, but some differences can be observed at the outlet of the bore. This means that the gaseous phase moved closer to the center of the bore.

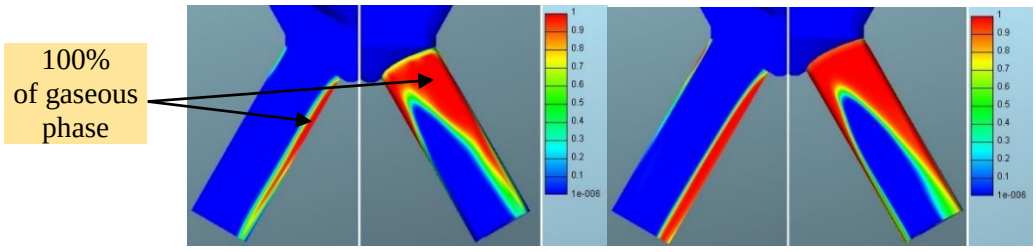

Fig. 16. Defined mass flow: Volume fraction of gaseous phase for mesh 1 (left) and mesh 2 (right)

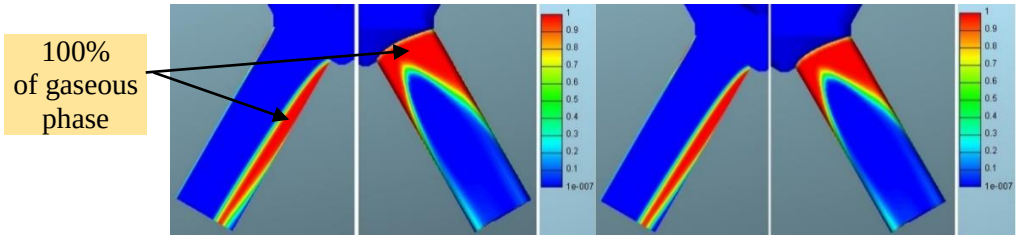

Fig. 17. Defined needle lift: Volume fraction of gaseous phase for for mesh 1 (left) and mesh 2 (right)

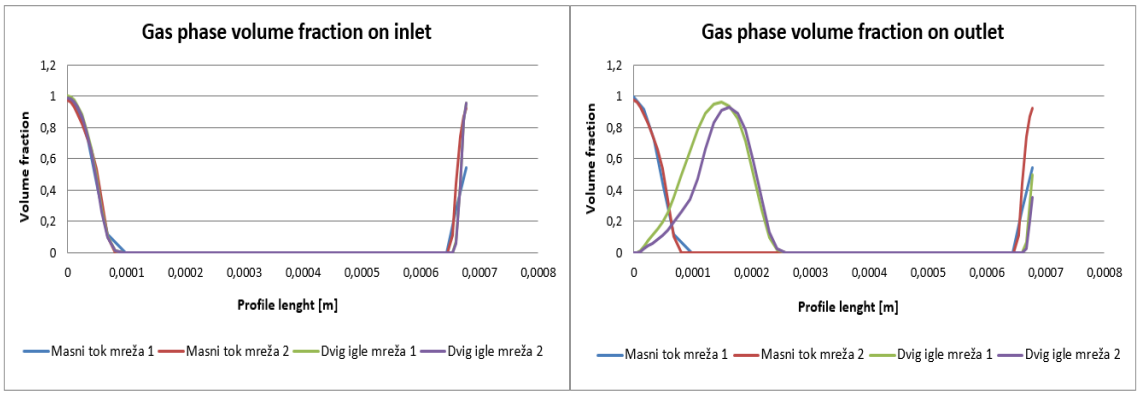

Fig. 18. The comparison of volume fraction (defined mass flow and needle lift) for meshes 1 and 2

4. CONCLUSIONS

In the field of computational fluid dynamics, there is still quite a lot of potential for improvement and innovation. Therefore, our research presents two different modes of injector nozzle simulation and we try to determine whether they are comparable or not. The first approach dealt with the defined time-dependent mass flow at the entrance to the injector, and the data were obtained experimentally. In the second case, the modelled calculations were replicated with the defined needle lift and the pressure at the inlet. Both were used at two different mesh volumes of numerical model.

It turned out that the approaches gave different results. The particularly large deviations occured in the calculated values of pressure and velocity. Much more comparable results were gained by turbulent kinetic energy and volume fractions.

It was also noted that the discrepancy was greater at the exit of the bore. In both approaches, partial reasons for the deviations resulted from in the inability of choice of exactly the same time interval, although measurement error was also possible. However, those factors could not be the cause of such large deviations in the case of pressure, especially because in the post-analysis, the possibility of incorrect settings in the control file was excluded.

Nevertheless, we managed to approximate the results in two ways. First, the inlet pressures were taken out of the results of simulation which was using the approach with the defined mass flow. This information was then set as a boundary condition in simulation, in which we defined the needle lift and pressure at the inlet. The match was much better. Therefore, we believed that with some adjustments of incoming data, especially with more accurately defined mass flow, we could achieve a very good match. Then we did the reverse, and from the simulation with the defined needle lift, the mass flows were received and were determined at the inlet. There was again a very good match in results.

Despite that, in the initial research phase, we could not confirm whether the approach was entirely comparable or not. We estimated that it would make sense to re-do the measurement of mass flow and needle lift, and after that simulations should be replicated with much more accurate mathematical analysis of physical conditions of the process, which would be subject to further consideration of the problem.

References

1. Kegl B. 2006. *Osnove motorjev z notranjim zgorevanjem.* [In Slovenien: *Fundamentals of internal combustion engines*]. Maribor: Fakulteta za strojništvo.
2. Volmajer M. 2001. „Numerična in eksperimentalna analiza tokovnih karakteristik vbrizgalne šobe dizelskega motorja". [In Slovenien: "Numerical and experimental analysis of flow characte9ristics of the injectors for diesel engines"]. MSc thesis. Maribor: TF.
3. Volmajer M. 2007. "Modeliranja večfaznih tokov v vbrizgalni šobi". [In Slovenian: "Modeling of multiphase flows in the injector"]. PhD thesis. Maribor: TF.
4. *Manual Fire*. AVL List GmbH. 2011. Graz.
5. *Turbulence modeling for beginners*. Tennessee: Tony Saad, University of Tennessee Space Institute. 2014. Available at: http://www.cfdonline.com/W/images/3/31/Turbulence_Modeling_For_Beginners.pdf.

Received 11.08.2015; accepted in revised form 21.12.2015